

Nucleophilic Substitution at Phosphorus Centers ($S_N2@P$)

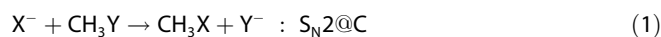
Marc A. van Bochove, Marcel Swart, and F. Matthias Bickelhaupt^{*[a]}

We have studied the characteristics of archetypal model systems for bimolecular nucleophilic substitution at phosphorus ($S_N2@P$) and, for comparison, at carbon ($S_N2@C$) and silicon ($S_N2@Si$) centers. In our studies, we applied the generalized gradient approximation (GGA) of density functional theory (DFT) at the OLYP/TZ2P level. Our model systems cover nucleophilic substitution at carbon in $X^- + CH_3Y$ ($S_N2@C$), at silicon in $X^- + SiH_3Y$ ($S_N2@Si$), at tricoordinate phosphorus in $X^- + PH_2Y$ ($S_N2@P3$), and at tetra-coordinate phosphorus in $X^- + POH_2Y$ ($S_N2@P4$). The main feature of going from $S_N2@C$ to $S_N2@P$ is the loss of the characteristic double-well potential energy surface (PES) involving a transition state $[X-CH_3-Y]^-$ and the occurrence of a single-well PES with a stable transition complex, namely, $[X-PH_2-Y]^-$ or $[X-POH_2-Y]^-$.

The differences between $S_N2@P3$ and $S_N2@P4$ are relatively small. We explored both the symmetric and asymmetric (i.e. $X, Y=Cl, OH$) S_N2 reactions in our model systems, the competition between backside and frontside pathways, and the dependence of the reactions on the conformation of the reactants. Furthermore, we studied the effect, on the symmetric and asymmetric $S_N2@P3$ and $S_N2@P4$ reactions, of replacing hydrogen substituents at the phosphorus centers by chlorine and fluorine in the model systems $X^- + PR_2Y$ and $X^- + POR_2Y$, with $R=Cl, F$. An interesting phenomenon is the occurrence of a triple-well PES not only in the symmetric, but also in the asymmetric $S_N2@P4$ reactions of $X^- + POCl_2-Y$.

Introduction

Bimolecular nucleophilic substitution (S_N2) is ubiquitous in organic chemistry.^[1] This holds, in particular, for nucleophilic substitution at carbon centers ($S_N2@C$), which—known for over 100 years^[2]—has been the subject of many experimental^[3] and theoretical studies.^[4] The nucleophilic substitution reaction between a halide anion and halomethane in the gas phase is generally used as an archetypal model for $S_N2@C$ [see Eq. (1)]:



This reaction proceeds preferentially through a backside nucleophilic attack of the halide anion at the carbon atom ($S_N2@C$), which goes with a concerted expulsion of the leaving group. A well-known feature of gas-phase $S_N2@C$ reactions is their double-well potential energy surface (PES) along the reaction coordinate^[3f,5] shown in Figure 1A for an identity reaction in which $X=Y$ (e.g. $Cl^- + CH_3Cl \rightarrow CH_3Cl + Cl^-$). This PES is characterized by two pronounced minima, associated with the reactant and product ion–molecule complexes (RC and PC) that are interconverted through the transition state (TS) for nucleophilic substitution at carbon. In the case of nonidentity reactions in which $X \neq Y$ (e.g. $Cl^- + CH_3Br \rightarrow CH_3Cl + Br^-$), the shape of the PES is strongly influenced by the reaction enthalpy. Usu-

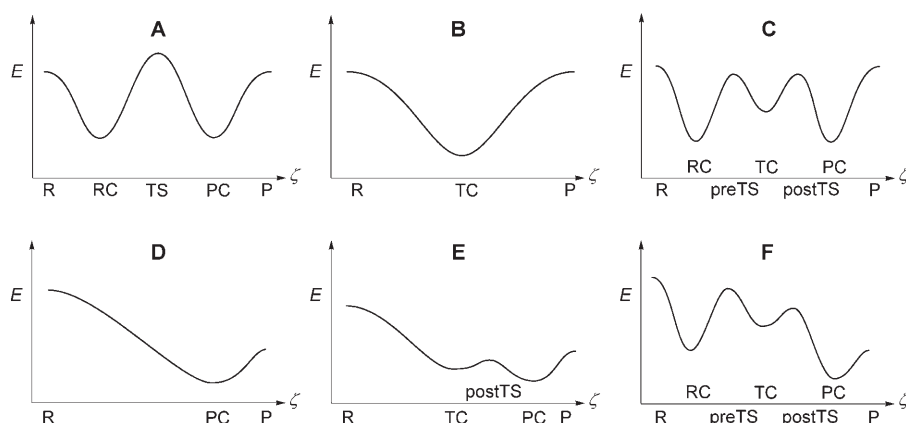


Figure 1. Types of potential energy surfaces (PESs) encountered in S_N2 reactions 1–8. R = reactants, RC = reactant complex, TS = transition state, TC = stable transition complex, PC = product complex, P = products.

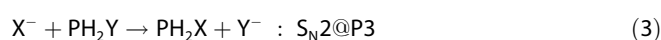
[a] M. A. van Bochove, Dr. M. Swart,⁺ Dr. F. M. Bickelhaupt
Theoretische Chemie
Scheikundig Laboratorium der Vrije Universiteit
De Boelelaan 1083, 1081 HV Amsterdam (The Netherlands)
Fax: (+31) 20-59 87629
E-mail: fm.bickelhaupt@few.vu.nl

[*] Current address:
Institut de Química Computacional
Universitat de Girona, Campus Montilivi
17071 Girona, Catalonia (Spain)
and
Institutió Catalana de Recerca i Estudis Avançats (ICREA)
08010 Barcelona, Catalonia (Spain)

Supporting information for this article is available on the WWW under <http://www.chemphyschem.org> or from the author.

ally, the central barrier encountered from RC to TS decreases with increasing exothermicity and eventually disappears completely for highly exothermic reactions (see Figure 1 D).

Whereas the $S_N2@C$ reaction has been extensively studied, much less investigations, both experimental and theoretical, have been devoted to studying the nature and mechanism of gas-phase nucleophilic substitution at other atoms, such as nitrogen,^[4g,6] silicon^[4b,7] and phosphorus.^[7b,8–10] Nucleophilic substitution at nitrogen centers appears to be very similar to $S_N2@C$ in the sense that it is associated with a double-well PES. On the other hand, a striking change in the nature of the reaction mechanism occurs for nucleophilic substitution at silicon and phosphorus atoms. An archetypal model for these reactions, namely, $S_N2@Si$ and $S_N2@P$, is the nucleophilic substitution between a halide anion and a halosilane or halophosphine [see Eqs. (2) and (3)]:

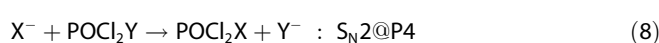
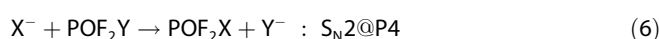


Note that this $S_N2@P3$ reaction is isoelectronic with—and structurally analogous to—the $S_N2@C$ and $S_N2@Si$ reactions of Equations (1) and (2), notwithstanding the obvious difference that the central, electrophilic atom in $S_N2@P3$ [Eq. (3)] is tri-coordinate (which is indicated with an affix “3” in our designation $S_N2@P3$) while that in $S_N2@C$ is tetracoordinate [Eq. (1)]. However, at variance with the latter, the $S_N2@P3$ reaction proceeds via a single-well PES (as shown in Figure 1 B), that is, it proceeds without encountering a first-order saddle point on the PES along the reaction coordinate.^[8] Thus, the transition structure $[X-PH_2-Y]^-$ of the $S_N2@P3$ reactions is not a transition state (TS) but instead a stable transition complex (TC). This behavior closely resembles that of nucleophilic substitution at silicon [Eq. (2)],^[7] and it is also observed in $S_N2@P4$ reactions involving a tetracoordinate central phosphorus atom [see Eq. (4)]:



One aspect that makes $S_N2@P$ reactions particularly interesting is their occurrence in various organic and biological processes that involve pentacoordinate phosphorus species.^[11] Yet, their nature has not been fully understood, in particular, whether they are stable, intermediate TCs or labile TSs. Recently, we showed how an increase in the coordination number of the central atom and the steric demand of the substituents leads to a stepwise shift of the $S_N2@P$ mechanism of symmetric reactions (i.e. $X=Y$) from a single-well potential (with a stable central TC), which is common for substitution at third-period atoms, to a triple-well potential (featuring a pre- and post-TS before and after the central TC), and back to a double-well potential (in which the pre- and post-barriers merge into one central TS); this double-well potential is well-known for substitution reactions at carbon.^[8a] Similar results were also obtained for $S_N2@Si$ reactions.^[7a] These results highlight the steric nature of the S_N2 barrier, but they also show how electronic effects modulate the barrier height.

Here, we extend our previous work on reactions 1–4 in three ways: i) we include the asymmetric reactions ($X \neq Y$) to probe, among others, if the phenomenon of triple-well PESs with pre- and post-transition states may also occur in exothermic or endothermic reactions; ii) we also examine the dependence of the reactions on the conformation of the reactants; and iii) we include studies of the frontside $S_N2@P$ reaction and other alternative pathways and compare these with the regular backside substitution. We have systematically explored all these issues in the symmetric and asymmetric $S_N2@C$, $S_N2@Si$, $S_N2@P3$, and $S_N2@P4$ reactions of Equations (1)–(8) (with affixes a, b, and c for $[X,Y]=[Cl,Cl]$, $[OH,OH]$ and $[OH,Cl]$, respectively).



Our explorations were carried out using the generalized gradient approximation (GGA) of density functional theory (DFT)^[12] at OLYP/TZ2P.^[13] This level of theory was previously shown to agree within a few kcal mol⁻¹ with highly correlated ab initio benchmarks.^[4b,14]

Interestingly, we can show that a triple-well PES, which features a stable pentavalent transition complex that is separated from stable reactant and product complexes, occurs not only for the thermoneutral symmetric $S_N2@P4$ reactions but also for endo- and exothermic asymmetric $S_N2@P4$ reactions.

Computational Methods

All calculations are based on density functional theory (DFT)^[12] and have been carried out with the Amsterdam density functional (ADF) program.^[15] Geometries and relative energies of the stationary points along the PESs of our model reactions as well as vibrational analyses thereof were computed with the generalized gradient approximation (GGA) of DFT using the OLYP functional which involves the optimized exchange (OPTX) functional proposed by Handy and coworkers,^[13b] and the Lee–Yang–Parr (LYP) correlation functional.^[13c] The OLYP functional was shown to lead to major improvements with respect to other GGA functionals for describing chemical reactions.^[16] In particular, the notorious underestimation of activation barriers is dramatically reduced.^[14,16a,17] Recently, we showed that OLYP agrees, within a few kcal mol⁻¹, with highly correlated ab initio benchmarks.^[4b,14]

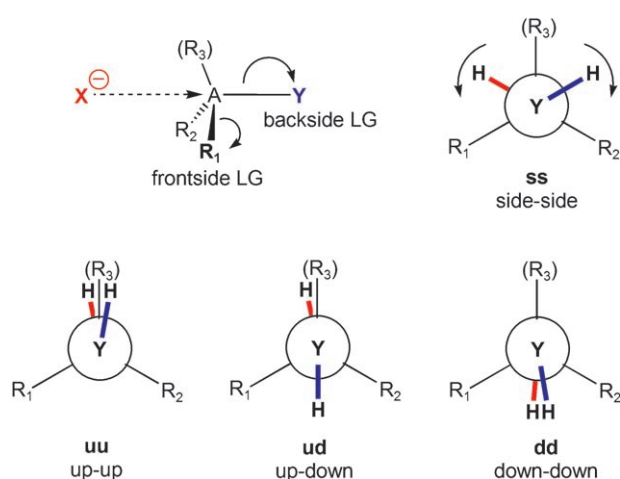
The OLYP functional was used in our computations in combination with the TZ2P basis set, which is a large uncontracted set of Slater-type orbitals (STOs) containing diffuse functions, which is of triple- ζ quality and has been augmented with two sets of polarization functions: $2p$ and $3d$ on hydrogen, $3d$ and $4f$ on carbon, oxygen, fluorine, silicon, phosphorus, and chlorine.^[15b,18] Note that no Gaussian basis functionals are involved. The core shells of carbon, oxygen, fluorine (1s), silicon, phosphorus, and chlorine ($1s^2 2p$) were treated by the frozen-core approximation.^[15b] An auxiliary set of s , p , d , f , and g STOs was used to fit the molecular density and to represent the Coulomb and exchange potentials accurately in each self-consistent field (SCF) cycle.^[15b,d] All stationary points were

confirmed to be equilibrium structures (no imaginary frequencies) or a transition state (one imaginary frequency) through vibrational analysis.^[19]

Results and Discussion

The results of our OLYP/TZ2P computations are collected in Tables 1–4 which contain key geometry parameters and relative energies. Additional data including Cartesian coordinates for all stationary points are available in Tables S1–S3 of the Supporting Information. There is a rich variation in structures, and Schemes 1 and 2 serve to summarize the required nomenclature. Scheme 1 defines the backside (Y^-) and frontside leaving group (R_1^-) and it serves to illustrate the various conformational variants that are possible if the nucleophile X^- and/or the leaving group Y^- are constituted by OH^- . Scheme 2 provides generic types of structures as they occur in the backside S_N2 pathways of reactions 1–8 as well as in alternative pathways, such as frontside S_N2 in which one of the substituents (i.e. R_1) act as a frontside leaving group. The various types of potential energy surfaces (PES) are schematically depicted in Figure 1.

In the following, we begin with a comparison and evaluation of the various symmetric and asymmetric backside S_N2 reactions (see Tables 1 and 2, Schemes 1 and 2, and Figure 1). Here, it should be noted that these reactions may proceed via different, although closely related, alternative pathways because of conformational isomerism, in the case that X^- and/or Y^- is hydroxide. The conformational isomerism that can (and does) occur in such instances is illustrated by the Newman projections in Scheme 1. For clarity, however, we first focus on the lowest-energy pathway of each of the backside S_N2 reactions. Later on, we extend our discussion to alternative backside S_N2 pathways, via conformationally different intermediates, as well as to competing frontside S_N2 processes.



Scheme 1. Nomenclature for the frontside (affix “-f” in the designation) and backside (not explicitly indicated) leaving groups and for various conformations in the case of OH nucleophiles and/or leaving groups ($A-R_3=C-R_3$, $Si-R_3$, P , or $P=O$).

Backside Substitution at Carbon

First, we examine the backside $S_N2@C$ reactions 1a–c. The symmetric reactions in which $X=Y$ are both either Cl^- (1a) or OH^- (1b) show, in agreement with previous reports,^[3,4] the characteristic double-well PES (see Figure 1A) where the reactant complex (RC) and the product complex (PC) are separated by a central barrier (with the TS on top) of about 9 and 16 kcal mol⁻¹ for 1a and 1b, respectively (see Table 1). Note that in the case of $X^- = OH^-$ (but not for $X^- = Cl^-$), the regular backside nucleophilic substitution is found to compete with facile alternative pathways. Notably, a proton transfer occurs from the substrate to the hydroxide anion; for example, the most stable encounter complex of $OH^- + CH_3OH$ is not the direct precursor of the S_N2 substitution reaction, namely, the reactant complex $OH^- \cdots CH_3OH$ (i.e. **1bRC** at -10.2 kcal mol⁻¹: this is a second-order saddle point on an enforced collinear approach with $\angle O-C-O$ fixed to 180°), but a methoxide–water complex (i.e. **1bWC** at -38.9 kcal mol⁻¹ relative to the reactants; structure type 1c in Scheme 2; see also Table S1 of the Supporting Information) that is formed through spontaneous proton transfer as OH^- approaches CH_3OH at the frontside.

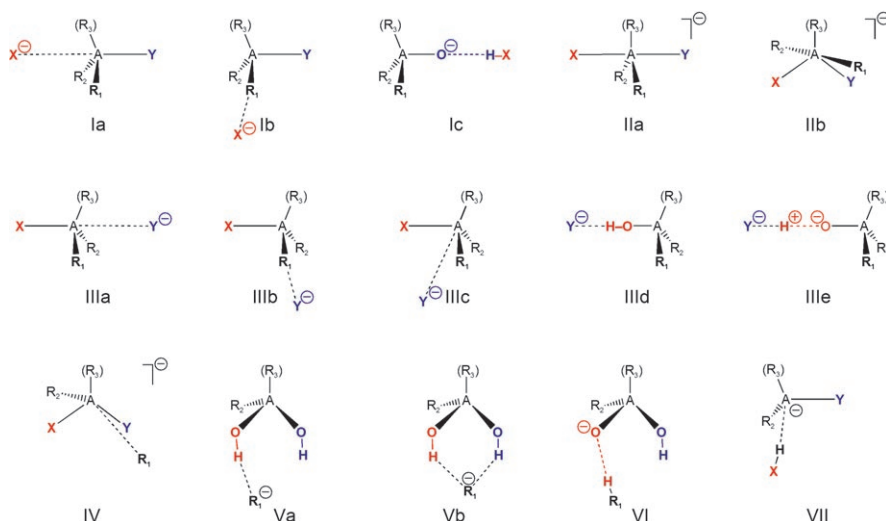
The asymmetric reaction 1c of $OH^- + CH_3Cl$ shows a barrierless expulsion of the chloride leaving group, if OH^- approaches the methyl group in a backside fashion within a reactive cone that is defined by a $Cl-C-[OH^-]$ angle of approximately 126° ,^[20] thus resulting in a single-well PES (see Figure 1D). The resulting product complex **1cPC** is found at -71.5 kcal mol⁻¹ relative to the reactants (see Table 1; structure type III d in Scheme 2). However, if the OH^- ion comes from outside the reactive cone, for example, in a frontside fashion, a reactant complex (**1cRC'**) is obtained at -20.4 kcal mol⁻¹ in which a hydrogen bond is formed between hydroxide and one of the methyl C–H bonds (structure type 1b in Scheme 2; see also Table S1 of the Supporting Information). The reactant complex **1cRC'** is separated from the reactive cone (and thus from **1cPC**) by a very small barrier of about 1 kcal mol⁻¹, which is associated with reaching the transition state **1cTS'** (see Table S1 of the Supporting Information).

The change from the typical double-well PES for reactions 1a–b (Figure 1A) to the single-well PES for reaction 1c (Figure 1D) is driven by a substantial exothermicity of reaction 1c which overall amounts to -56.5 kcal mol⁻¹ (see Table 1). Note that this is practically identical to the difference in proton affinities, that is, -56.4 kcal mol⁻¹,^[21] between nucleophile (OH^-) and leaving group (Cl^-). The expelled Cl^- leaving group migrates around the resulting methanol to form the $Cl^- \cdots HOCH_3$ product complex (**1cPC**) in which chloride hydrogen binds by -15 kcal mol⁻¹ to the hydroxy group (structure type III d in Scheme 2).

In the $S_N2@C$ reactions involving hydroxide as the nucleophile or the leaving group (i.e. 1b and 1c), the orientation of the OH group(s) in the stationary points associated with the pathway of the backside attack is in all cases “d” (see Scheme 1 and Table 2). This appears to be so irrespective of the initial orientation in the reactants as they approach each other. Thus, the OH group is always oriented staggered with

No.	Reaction	Shape of the PES ^[b]	RC	preTS	TS/TC	postTS	PC	P
1 a	Cl ⁻ + CH ₃ Cl	double well (A)	-9.02	-	-0.14	-	-9.02	0.00
1 b	OH ⁻ + CH ₃ OH	double well (A)	-10.17 ^[c]	-	6.16	-	-10.17 ^[c]	0.00
1 c	OH ⁻ + CH ₃ Cl	single well (D)	-	-	-	-	-71.54	-56.51
2 a	Cl ⁻ + SiH ₃ Cl	single well (B)	-	-	-24.43	-	-	0.00
2 b	OH ⁻ + SiH ₃ OH	single well (B)	-	-	-53.79	-	-	0.00
2 c	OH ⁻ + SiH ₃ Cl	single well (B)	-	-	-71.04	-	-	-60.58
3 a	Cl ⁻ + PH ₂ Cl	single well (B)	-	-	-26.17	-	-	0.00
3 b	OH ⁻ + PH ₂ OH	single well (B)	-	-	-40.19	-	-	0.00
3 c	OH ⁻ + PH ₂ Cl	single well (B)	-	-	-68.28	-	-	-58.00
4 a	Cl ⁻ + POH ₂ Cl	single well (B)	-	-	-22.33	-	-	0.00
4 b	OH ⁻ + POH ₂ OH	single well (B)	-	-	-48.78	-	-	0.00
4 c	OH ⁻ + POH ₂ Cl	single well (D)	-	-	-	-	-79.68	-67.52
5 a	Cl ⁻ + PF ₂ Cl	single well (B)	-	-	-24.74	-	-	0.00
5 b	OH ⁻ + PF ₂ OH	single well (B)	-	-	-45.49	-	-	0.00
5 c	OH ⁻ + PF ₂ Cl	single well (B)	-	-	-75.87	-	-	-67.87
6 a	Cl ⁻ + POF ₂ Cl	single well (B)	-	-	-13.62	-	-	0.00
6 b	OH ⁻ + POF ₂ OH	single well (B)	-	-	-54.17	-	-	0.00
6 c	OH ⁻ + POF ₂ Cl	double well (E)	-	-	-73.44	-73.32	-76.13	-72.34
7 a	Cl ⁻ + PCl ₂ Cl	single well (B)	-	-	-23.27	-	-	0.00
7 b	OH ⁻ + PCl ₂ OH	single well (B)	-	-	-51.99	-	-	0.00
7 c	OH ⁻ + PCl ₂ Cl	single well (B)	-	-	-75.34	-	-	-66.71
8 a	Cl ⁻ + POCl ₂ Cl	triple well (C)	-17.48	-2.04	-8.43	-2.04	-17.48	0.00
8 b	OH ⁻ + POCl ₂ OH	triple well (C)	-34.48	[d]	-58.02 ^[e]	[d]	-34.48	0.00
8 c	OH ⁻ + POCl ₂ Cl	triple well (F)	-44.71	[d]	-70.25	-68.19	-82.28	-70.93

[a] Computed at the OLYP/TZ2P level. See Schemes 1 and 2 for schematic structures and definitions. See Table 2 for geometry parameters. [b] Shape of the potential energy surface (PES): either single well (no TS), double well (one TS), or triple well (two TS); the PES type, as depicted in Figure 1, is shown in parenthesis. [c] Labile with respect to forming the water-methoxide complex **1bWC** (see text). [d] Not found because of a nonconverging SCF procedure. [e] TC along the enforced backside S_N2@P reaction coordinate 8b with uu configuration (see Scheme 1). This species is, however, a TS for a symmetric frontside S_N2@P substitution of Cl⁻ + POCl(OH)₂, thereby leading to the expulsion of Cl⁻.



Scheme 2. Generic structures I–VII of stationary points along backside and alternative frontside S_N2 pathways (the nucleophile X is represented by red, the leaving group Y is shown in blue, and the frontside leaving group R₁ is shown in bold black (A–R₃ = C–R₃, Si–R₃, P, or P=O; R₁, R₂ = H, F, Cl; see also Scheme 1). For the geometry parameters see Tables 2 and 4.

respect to the methyl C–H bonds (reactions 1 b and 1 c) and *cis* with respect to a second O–H bond (reaction 1 b).

stituents X,Y=Cl occupy the axial positions (type IIa in Scheme 2). In **2bTC**, however, the electronegative substituents X,Y=OH adopt equatorial positions (type IIb in Scheme 2).

Backside Substitution at Silicon

As pointed out in the introduction, the archetypal reactions of X⁻ + CH₃X and X⁻ + SiH₃X are often employed to illustrate how the reaction profile changes from a double-well PES, involving a central TS for substitution at a second-period atom (S_N2@C), to a single-well PES associated with a stable TC for substitution at the third-period congener (S_N2@Si).^[4b,7a] Indeed, the symmetric X⁻ + SiH₃X reactions 2a and 2b, in which X=Cl and OH, respectively, have a single-well PES (see Figure 1B) with barrierless formation of a stable central transition complex (TC) at -24 and -54 kcal mol⁻¹ for **2aTC** and **2bTC**, respectively. In **2aTC** the electronegative substituents X,Y=Cl occupy the axial positions (type IIa in Scheme 2). In **2bTC**, however, the electronegative substituents X,Y=OH adopt equatorial positions (type IIb in Scheme 2).

Table 2. Geometry parameters [\AA , degrees] for stationary points of $S_{\text{N}}2$ reactions 1–8.^[a]

Species	Type ^[b]	$R_{1,2}$ ^[c]	Conformation ^[d]	X-A	A-Y	A-R ₁ ^[e]	X-R ₁ ^[f]	Y-R ₁ ^[f]	X-R ₃ ^[f]	Y-R ₃ ^[f]	X-A-Y
1aRC	Ia	H	–	3.37	1.84	1.09	3.20	2.41	3.20	2.41	180
1aTS	Ila	H	–	2.35	2.35	1.07	2.59	2.59	2.59	2.59	180
1bRC ^[g]	Ia	H	dd	3.24	1.46	1.10	2.99	2.14	3.10	2.06	180
1bTS	Ila	H	dd	1.97	1.97	1.08	2.26	2.26	2.21	2.21	184
1cPC	IIId	H	d	1.40	3.72	1.11	2.10	3.73	2.04	4.78	54
2aTC	Ila	H	–	2.36	2.36	1.49	2.78	2.78	2.78	2.78	180
2bTC	IIb	H	ss	1.74	1.74	1.59	2.31	2.36	2.80	2.80	126
2cTC	Ila	H	d	1.77	2.58	1.50	2.50	2.82	2.37	2.81	184
3aTC	Ila	H	–	2.42	2.42	1.42	2.75	2.75	–	–	172
3bTC(uu)	Ila	H	uu	1.92	1.92	1.42	2.33	2.33	–	–	171
3cTC(u)	Ila	H	u	1.79	2.74	1.42	2.36	2.86	–	–	171
4aTC	Ila	H	–	2.37	2.37	1.40	2.61	2.61	3.05	3.05	156 ^[h]
4bTC(uu)	Ila	H	uu	1.80	1.80	1.42	2.18	2.18	2.26	2.26	166
4cPC(u)	IIIb	H	u	1.65	3.57	1.45	2.41	2.16	2.58	4.67	103
5aTC	Ila	F	–	2.40	2.40	1.62	2.91	2.91	–	–	182
5bTC(dd)	Ila	F	dd	1.80	1.80	1.69	2.44	2.44	–	–	177
5cTC(d)	Ila	F	d	1.71	2.72	1.64	2.45	3.11	–	–	182
6aTC	Ila	F	–	2.27	2.27	1.60	2.70	2.70	2.84	2.84	168
6bTC(uu)	Ila	F	uu	1.73	1.73	1.64	2.32	2.32	2.10	2.10	170
6cTC(u)	Ila	F	u	1.69	2.44	1.60	2.34	2.74	2.22	2.88	169
6c-postTS(u)	IIla	F	u	1.64	3.23	1.56	2.41	3.16	2.42	3.43	165
6cPC(u)	IIIc	F	u	1.58	4.07	1.56	2.48	3.77	2.60	5.53	58
7aTC	Ila	Cl	–	2.42	2.42	2.11	3.32	3.32	–	–	192
7bTC(dd)	Ila	Cl	dd	1.75	1.76	2.29	2.77	2.77	–	–	171
7cTC(d)	Ila	Cl	d	1.70	2.71	2.15	2.85	3.47	–	–	188
8aRC	Ib	Cl	–	4.80	2.09	2.06	2.74	3.32	5.64	2.97	107
8a-preTS	Ia	Cl	–	3.27	2.12	2.03	3.44	3.11	3.45	2.89	170
8aTC	Ila	Cl	–	2.30	2.30	2.10	3.04	3.04	2.84	2.84	170
8bRC(uu)	Ib	Cl	uu	4.31	1.65	2.14	2.17	3.01	5.17	2.49	103
8bTC(uu) ^[i]	Ila	Cl	uu	1.71	1.71	2.19	2.69	2.69	2.12	2.12	167
8cRC(u)	Ib	Cl	u	4.28	2.15	2.18	2.10	3.52	5.05	2.99	110
8cTC(u)	Ila	Cl	u	1.70	2.39	2.13	2.69	3.07	2.18	2.85	169
8c-postTS(u)	IIla	Cl	u	1.66	3.09	2.05	2.76	3.36	2.34	3.29	170
8cPC(u)	IIIb	Cl	u	1.63	4.88	2.02	2.88	2.86	2.52	5.76	102

[a] Computed at the OLYP/TZ2P level. See Table 1 for relative energies. [b] Generic types of stationary points (see Scheme 2). [c] See Scheme 1 for a perspective that defines R_1 and R_2 . [d] Orientation of hydroxyl protons: u = up, d = down, s = sideways (see Scheme 1). [e] A-R₁ may differ from A-R₂ if X[–] or Y[–] interact only with R₁. [f] For X, Y = OH, the shortest [OH]–R distance is given, that is, either O–R or H–R. [g] Labile with respect to the formation of the water–methoxide complex **1bWC** (see text). [h] This value was previously published (erroneously) to be 114° (see ref. [8a]). [i] See footnote “e” of Table 1.

The reactants $\text{OH}^- + \text{SiH}_3\text{OH}$ of the symmetric $S_{\text{N}}2@Si$ reaction 2b can also combine and form, via barrierless proton transfer, a water complex $\text{SiH}_3\text{O}^-\cdots\text{H}_2\text{O}$ (**2bWC**) which is about 5 kcal mol^{-1} more stable than the TC (structure type Ic in Scheme 2; see also Table S1 of the Supporting Information). This behavior resembles that of the corresponding $S_{\text{N}}2@C$ reaction 1b of $\text{OH}^- + \text{CH}_3\text{OH}$ (see above). A difference with the $S_{\text{N}}2@C$ reaction is however that **2bWC** is only formed if hydroxide approaches silanol at the hydroxy side, whereas **1bWC** is formed spontaneously in any (unconstrained) encounter of OH^- and CH_3OH , no matter if hydroxide starts its approach from the methyl or the hydroxy side of methanol.

The asymmetric $S_{\text{N}}2@Si$ reaction 2c of $\text{OH}^- + \text{SiH}_3\text{Cl}$ is again associated with a single-well PES featuring a stable TC (**2cTC**) at $-71 \text{ kcal mol}^{-1}$ (see Table 1). The exothermicity of the reaction is substantial and amounts to $-61 \text{ kcal mol}^{-1}$. The fact that we deal with a pentavalent TC, **2cTC**, (Figure 1B) rather than with an asymmetric product complex, which results from a barrierless expulsion of the Cl^- leaving group (Figure 1D), be-

comes clear if we carefully examine the key geometry parameters in Table 2: the O–Si and Si–Cl distances of 1.77 and 2.58 \AA , respectively, may suggest—at first sight—that we have a PC with an expelled Cl^- leaving group. However, comparison with the corresponding O–Si distance in **2bTC** (1.74 \AA) and the Si–Cl distance in **2aTC** (2.36 \AA) shows that the values in the asymmetric **2cTC** only moderately deviate from those in a symmetric pentavalent TC (see Table 2 and structure type Ila in Scheme 2). The species **2cTC** can either dissociate directly to the products $\text{SiH}_3\text{OH} + \text{Cl}^-$ or rearrange into a stable alternative product complex in which chloride forms a hydrogen bond with the hydroxyl group of silanol (see **2cPC-alt** in Table S1 of the Supporting Information).

In the $S_{\text{N}}2@Si$ reactions involving hydroxide as the nucleophile or the leaving group (i.e., 2b and 2c), the OH group(s) in the transition complex only adopt one conformation, irrespective of the initial orientation in the reactants, as they approach each other, namely, “ss” for **2bTC** and “d” for **2cTC** (see Scheme 1 and Table 2). Thus, the OH groups in **2bTC** are ori-

ented parallel to two of the Si–H bonds (those which have adopted axial positions, see above), whereas the OH-group conformation in **2cTC** is staggered with respect to the silyl Si–H bonds. The situation in the $S_N2@Si$ reactions 2b and 2c, where only one conformation of OH groups exists in the stationary points, resembles the behavior in the corresponding $S_N2@C$ reactions 1b and 1c.

Backside Substitution at Phosphorus

The symmetric nucleophilic substitutions at tricoordinate ($S_N2@P3$, reactions 3a and 3b) and tetracoordinate phosphorus ($S_N2@P4$, reactions 4a and 4b) proceed via the barrierless formation of a hypervalent transition complex in a single-well PES, much like the corresponding $S_N2@Si$ reactions 2 (see Table 1 and Figure 1B). This similarity between the PESs of $S_N2@P$ and $S_N2@Si$ agrees well with previous reports from our group and from other researchers.^[6] However, we also find a new feature in the $S_N2@P$ reactions, namely, the existence (for a given set of reactants) of multiple pathways which differ from each other in the OH-group conformation (see below).

The symmetric $S_N2@P3$ reactions 3a and 3b yield the transition complexes **3aTC** and **3bTC(uu)**—both with a structure type IIa—at -26.2 and -40.2 kcal mol⁻¹, respectively (see Scheme 2 and Table 1). Note that the transition complex **3bTC(uu)** of the reaction between OH⁻ and **3bR(u)** (i.e. PH₂OH with OH “up”, see Scheme 1) is associated with the lowest energy but is not the only pathway. Alternative pathways exist, with the OH-group conformations “ud” and “dd” and the transition complexes **3bTC(ud)** and **3bTC(dd)**, which are slightly higher in energy, that is, by 1.2 and 2.4 kcal mol⁻¹, respectively, than **3bTC(uu)** (see Table S1 of the Supporting Information).

By introducing the phosphoryl oxygen, that is, by going from the $S_N2@P3$ reactions 3a and 3b to the corresponding $S_N2@P4$ reactions 4a and 4b, transition complexes are obtained that are slightly destabilized (by 4 kcal mol⁻¹) in the case of **4aTC** and stabilized (by 9 kcal mol⁻¹) in the case of **4bTC(uu)** (see Table 2; structure type IIa in Scheme 2). The slight destabilization of **4aTC** relative to **3aTC** is ascribed to the higher extent of steric crowding associated with going from tetracoordination in the latter to pentacoordination in the former transition complex (see ref. [8a]). The higher extent of steric congestion in reactions 4a and 4b is also suggested by the somewhat smaller X–P–Y angles in **4aTC** and **4bTC(uu)** (156 and 166°) compared to those of **3aTC** and **3bTC** (172 and 171°, respectively, see Table 2).

The stabilization (by 9 kcal mol⁻¹) of **4bTC(uu)** relative to **3bTC(uu)** can be ascribed to the formation of hydrogen bonds in the former between the phosphoryl oxygen and each of the two OH groups pointing “up”, that is, towards this negatively charged oxygen atom (see Scheme 1). Interestingly, the energy rises only about 1 kcal mol⁻¹ upon going to the **4bTC2(ss)** conformer in which the OH groups are oriented sideways, pointing toward the same hydrogen substituent at the phosphorus center (structure type IIb in Scheme 2; see also Table S1 of the Supporting Information). This result suggests dihydrogen bonding (DHB)^[22] in **4bTC2(ss)** between the protonic hydrogen

in the OH groups and the (slightly) hydridic hydrogen substituent at the phosphorus center. We note that **4bTC2(ss)** occurs as an intermediate in side reactions of the backside $S_N2@P4$ process 4b (see below; see also Tables 3 and 4).

Also, the asymmetric $S_N2@P$ reactions 3c and 4c both proceed via single-well PESs, but the character of the equilibrium structure in the potential energy well of OH⁻ + PH₂Cl ($S_N2@P3$, reaction 3c) differs from that of OH⁻ + POH₂Cl ($S_N2@P4$, reaction 4c). In the former, we have a hypervalent transition complex **3cTC(u)** at -68 kcal mol⁻¹, with O–P and P–Cl bond distances of 1.79 and 2.74 Å, respectively (see Figure 1B; structure type IIa in Scheme 2), that is, only slightly contracted and expanded, respectively, compared to the corresponding values in **3bTC(uu)** and **3aTC** (see Tables 1 and 2). This resembles the nature of the corresponding $S_N2@Si$ reaction 2c of OH⁻ + SiH₃Cl (see above). Dissociation of **3cTC(u)** leads to the formation of the products **3cP(u)** + Cl⁻, that is, PH₂OH with OH in the “up” conformation (see Scheme 1). Overall, reaction 3c is exothermic by -58 kcal mol⁻¹ (see Table 1).

On the other hand, the asymmetric $S_N2@P4$ substitution of OH⁻ + POH₂Cl (reaction 4c) shows a barrierless expulsion of the chloride leaving group, if the OH⁻ ion approaches the POH₂ group in a backside fashion within a reactive cone that is defined by a Cl–P–[OH⁻] angle of roughly 97°, ^[20] thus resulting in a single-well PES (see Figure 1D). The resulting product complex **4cPC(u)** is found at -80 kcal mol⁻¹ relative to the reactants and contains a hydrogen bond between Cl⁻ and a P–H bond, namely, Cl⁻⋯H–P(O)(OH)H (see Figure 1D; structure type IIIb in Scheme 2; see also Tables 1 and 2). However, if the OH⁻ species approaches from outside this reactive cone, for example, in frontside fashion, a spontaneous proton abstraction from POH₂Cl takes place, with formation of the H–O–H⋯POHCl water complex **4cWC** at -73.8 kcal mol⁻¹ (structure type VII in Scheme 2; see also Table S1 of the Supporting Information). The absence of a transition complex and the spontaneous formation of a product complex **4cPC(u)** resembles the situation of the corresponding $S_N2@C$ reaction 1c of OH⁻ + CH₃Cl (see above), which also proceeds via an asymmetric single-well PES (as shown in Figure 1D). Dissociation of **4cPC(u)** leads to the products **4cP(u)** + Cl⁻, that is, POH₂OH, with OH in the “up” conformation (see Scheme 1). Overall, reaction 4c is exothermic by -67.5 kcal mol⁻¹ (see Table 1).

Chlorine-Substituent Effects on $S_N2@P$

As pointed out above, the introduction of an extra (oxygen) substituent at the phosphorus center, from the tetracoordinate **3aTC** to the pentacoordinate **4aTC**, causes a slight destabilization (of about 4 kcal mol⁻¹) of the transition complex, which is caused by an increase in steric congestion (see Table 1 and ref. [8a]). Likewise, replacing the hydrogen atoms on the phosphorus center by the more bulky chlorine atoms, from the tetracoordinate **3aTC** to the pentacoordinate **7aTC**, destabilizes the transition complex again by a comparatively small amount (ca. 3 kcal mol⁻¹, see Table 1). In line with the increased steric demand of the chlorine substituents, the X–P–Y angle increases from 172° in **3aTC** (i.e. axial nucleophile and leaving group

Table 3. Relative energies [kcal mol⁻¹] for stationary points along the PES of regular backside S_N2@P (back), frontside S_N2@P (front), and alternative frontside S_N2@P + elimination (alt) reactions starting from the central transition complexes (TC) with OH⁻ as the attacking nucleophile.^[a]

No.	Reaction	Path	TC ΔE	TC Name	TS ΔE	TS Name	Intermediate ΔE	Intermediate Name	TS ΔE	TS Name	PC ΔE	PC Name	Products ΔE	Products Name
3b	OH ⁻ + 3bR(u)	back	-40.19	3bTC(uu)	-	-	-	-	-	-	-	0.00	3bP(u) + OH ⁻	
		front	-40.19	3bTC(uu)	-4.28	3bTS(uu)-f ^[b]	-	-	-	-	-56.64	3bPC-f	2.30	3bP-f + H ⁻
		alt	-40.19	3bTC(uu)	-4.28	3bTS(uu)-f ^[b]	-	-	-	-	-56.64	3bPC-f	-53.97	3bP-f/alt + H ₂
4b	OH ⁻ + 4bR(u)	back	-48.78	4bTC(uu)	-	-	-	-	-	-	-	0.00	4bP(u) + OH ⁻	
		front	-48.78	4bTC(uu)	-46.89	4bTS1(ss)-f	-48.04	4bTC2(ss)-f	-38.34	4bTS2(ss)-f	-83.11	4bPC-f	-8.09	4bP-f + H ⁻
		alt	-48.78	4bTC(uu)	-46.89	4bTS1(ss)-f	-48.04	4bTC2(ss)-f	-38.34	4bTS2(ss)-f	-83.11	4bPC-f	-81.78	4bP-f/alt + H ₂
5b	OH ⁻ + 5bR(d)	back	-45.49	5bTC(dd)	-	-	-	-	-	-	-	0.00	5bP(d) + OH ⁻	
		front	-45.49	5bTC(dd)	-35.85	5bTS(dd)-f	-	-	-	-	-80.14	5bPC-f	-13.16	5bP-f + F ⁻
		alt	-45.49	5bTC(dd)	-35.85	5bTS(dd)-f	-	-	-	-	-80.14	5bPC-f	-57.56	5bP-f/alt + HF
6b	OH ⁻ + 6bR(u)	back	-54.17	6bTC(uu)	-	-	-	-	-	-	-	0.00	6bP(u) + OH ⁻	
		front	-54.17	6bTC(uu)	-25.02	6bTS(u)-f ^[d]	-	-	-	-	-93.14	6bPC-f	-17.89	6bP-f + F ⁻
		alt	-54.17	6bTC(uu)	-25.02	6bTS(u)-f ^[d]	-	-	-	-	-93.14	6bPC-f	-73.55	6bP-f/alt + HF
6c	OH ⁻ + 6cR	back	-73.44	6cTC(u)	-73.32	6c-postTS(u)	-	-	-	-	-76.13	6cPC(u)	-72.34	6cP(u) + Cl ⁻
		front	-73.44	6cTC(u)	-69.98	6cTS1(s)-f	-73.34	6cTC2(s)-f	-69.04	6cTS2(s)-f	-103.11	6cPC-f	-19.17	6cP-f + F ⁻
		alt	-73.44	6cTC(u)	-69.98	6cTS1(s)-f	-73.34	6cTC2(s)-f	-69.04	6cTS2(s)-f	-103.11	6cPC-f	-86.28	6cP-f/alt + HF
7b	OH ⁻ + 7bR(d)	back	-51.99	7bTC(dd)	-	-	-	-	-	-	-100.15	7bPC(η ³)-f ^[d]	0.00	7bP(d) + OH ⁻
		front	-51.99	7bTC(dd)	-51.72	7bTS(dd)-f	-	-	-	-	-100.15	7bPC(η ³)-f ^[d]	-64.16	7bP-f + Cl ⁻
		back'	-88.85	7bTC-alt ^[e]	-	-	-	-	-	-	-	-	-	-
7b'	OH ⁻ + 7bR(s)	front'	-88.85	7bTC-alt ^[e]	-88.66	7bTS-f/alt	-	-	-	-	-97.19	7bPC(η ³)-f	-67.05	7bP-f/alt + Cl ⁻
		back	-88.85	7bTC-alt ^[e]	-	-	-	-	-	-	-102.93	7bPC(η ³)-f ^[f]	-66.94	7bP-f + Cl ⁻
		front'	-88.85	7bTC-alt ^[e]	-	-	-	-	-	-	-102.93	7bPC(η ³)-f ^[f]	-66.94	7bP-f + Cl ⁻
8b	OH ⁻ + 8bR(u)	back	-58.02	8bTC(uu) ^[g]	-	-	-105.36	8bPC(η ³)-f ^[h]	-103.95	8bTS(η ³ /η ³)-f	-113.51	8bPC(uu)	0.00	8bP(u) + OH ⁻
		back'	-	-	-	-	-	-	-	-	-34.48	8bPC(uu)	0.00	8bP(u) + OH ⁻
		front	-	-	-	-	-	-	-	-	-113.51	8bPC(η ³)-f ^[h]	-70.17	8bP-f + Cl ⁻
8c	OH ⁻ + 8cR	back	-70.25	8cTC(u)	-68.19	8c-postTS(u)	-	-	-	-	-105.36	8bPC(η ³)-f ^[h]	-71.03	8bP-f/alt + Cl ⁻
		front	-70.25	8cTC(u)	-69.69	8cTS(s)-f	-	-	-	-	-82.28	8cPC(u)	-70.93	8cP(u) + Cl ⁻
		back	-70.25	8cTC(u)	-69.69	8cTS(s)-f	-	-	-	-	-111.89	8cPC-alt	-70.29	8cP(d) + Cl ⁻

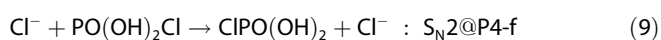
[a] Computed at the OLYP/7Z2P level. See Schemes 1 and 2 for schematic structures and definitions. See Table 4 for geometry parameters. [b] Second-order saddle point.^[25] [c] The imaginary normal mode of this TS involves turning a hydrogen atom in the direction of the expelled F⁻ ion instead of a movement related to the P–F distance. [d] Other conformations different to the dd one [which leads from 7bR(d) to 7bTC(d)] show a barrierless formation of this PC. [e] Formation of the complex 7bTC-alt is observed when 7bR(s) is approached by an incoming, s-oriented OH⁻ group that points to an opposite direction than that of the OH group in the substrate (see Scheme 1). [f] Spontaneous formation of 7bPC(η³)-f for all orientations of the incoming OH⁻ group, except for one. [g] TC along the enforced backside S_N2@P reaction coordinate 8b with uu configuration (see Scheme 1). Note, however, that this conformation of 8bTC (namely, uu) as well as all other conformations (i.e., ud, du, dd) correspond to a TS for a symmetric frontside S_N2@P substitution of Cl⁻ + POC(OH)₂, thereby leading to the expulsion of Cl⁻. [h] Not found because of a nonconverging SCF procedure. [i] In the case of the du-conformation, that is, a d-oriented OH⁻ attacking the species 8bR(u); also in the case of a ud-conformation, not shown in the table. [j] Formed (barrierless) from the dd and uu conformations (see also footnote "g").

slightly pointing down to the equatorial hydrogen substituents) to 192° in **7aTC** (i.e. axial nucleophile and leaving group slightly pointing up, away from the equatorial chlorine substituents; structure type IIa in Scheme 2; see also Table 2).

More drastic changes occur from the symmetric $S_N2@P3$ reaction 3a of $Cl^- + PH_2Cl$ to the $S_N2@P4$ reaction 8a of $Cl^- + POCl_2Cl$, along which both the coordination number at the phosphorus center and the steric bulk of the substituents R_1 and R_2 increase (see Scheme 1). Thus, if we go from **3aTC** to **8aTC**, the transition complex is significantly destabilized (by about 18 kcal mol^{-1} , see Table 1). The $X-P-Y$ angle remains essentially unchanged (it varies from 172 to 170°), in line with the more evenly distributed rise in steric demand around the central phosphorus atom (structure type IIa in Scheme 2; see also Table 2). In addition, the nucleophile and leaving group must now penetrate a steric barrier provided by the three substituents before they can bind to or leave the central phosphorus atom (see below). This gives rise to a qualitative change in the character of the reaction profile from a single- to a triple-well PES (see Figure 1B,C). The latter PES features steric pre- and post-transition states (**8a-preTS** and **8a-postTS** at $-2.0 \text{ kcal mol}^{-1}$, structure types Ia and IIIa, respectively) that separate the stable transition complex **8aTC** (at $-8.4 \text{ kcal mol}^{-1}$, structure type IIa) by a barrier of $6.4 \text{ kcal mol}^{-1}$ from the more stable (by $9.1 \text{ kcal mol}^{-1}$) reactant and product complexes **8aRC** and **8aPC** (found at $-17.5 \text{ kcal mol}^{-1}$, structure types Ib and IIIb; see Tables 1 and 2, and Scheme 2). Note that there is now an intrinsic barrier of more than 15 kcal mol^{-1} associated with reaching the transition complex from the reactant complex (see Table 1).

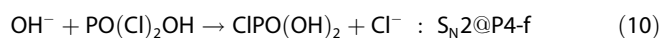
Also, in the case of the symmetric $S_N2@P4$ reaction 8b of $OH^- + POCl_2OH$, a triple-well PES occurs as a result of the increased steric congestion around the central phosphorus atom (see below). Here, however, the reactant and product complexes **8bRC(uu)** and **8bPC(uu)** (at $-34.5 \text{ kcal mol}^{-1}$, structure types Ib and IIIb) as well as the transition complex **8bTC(uu)** (at $-58.0 \text{ kcal mol}^{-1}$, structure type IIa) are significantly more stable than in the reaction 8a of $Cl^- + POCl_2Cl$ (see Tables 1 and 2, and Scheme 2). This holds, in particular, for **8bTC(uu)**, which is even more stable than the reactant complexes, at variance with the situation for **8aTC**. The enhanced stability of **8bTC(uu)** can be largely ascribed to the two hydrogen bonds between the phosphoryl oxygen and the two OH groups that are pointing "up" and towards this oxygen atom (see Scheme 1). This intramolecular hydrogen bonding is similar to that in **4bTC(uu)**.

However, unlike the other stationary points, **8bTC(uu)** is stable only along an enforced backside- S_N2 reaction coordinate 8b. This species is, in fact, labile with respect to the expulsion of a chloride anion and corresponds to the transition state for the frontside $S_N2@P4$ reaction of $Cl^- + PO(OH)_2Cl$ (designated by $S_N2@P4-f$) shown in Equation (9):



Note that this implies that when proceeding from the reactants $OH^- + PO(Cl)_2OH$ and approaching the saddle point of

8bTC(uu), the process will deviate from the straight backside $S_N2@P4$ path of reaction 8b and enter into the channel of reaction 9, thus leading to the same products as the latter. Overall, this yields the frontside $S_N2@P4-f$ reaction shown in Equation (10):



Next, we address the question whether the triple-well character of the PES (see Figure 1C) is robust towards introducing an asymmetry by making the reaction exothermic. In the case of the $S_N2@C$ reactions 1, for example, we have seen how a central barrier of 9 kcal mol^{-1} can disappear if we go from the thermoneutral reaction 1a of $Cl^- + CH_3Cl$ to the ($-57 \text{ kcal mol}^{-1}$) exothermic reaction 1c of $OH^- + CH_3Cl$ (see above). Likewise, if we go from the symmetric, thermoneutral $S_N2@P4$ reaction 8a of $Cl^- + POCl_2Cl$ to the asymmetric reaction 8c of $OH^- + POCl_2Cl$, we introduce an even larger exothermicity of $-71 \text{ kcal mol}^{-1}$ (see Table 1). Interestingly, although the reaction profile becomes asymmetric, the triple-well nature of the PES is preserved, that is, we go from the PES-type in Figure 1C to that in Figure 1F. Thus, we have a reactant complex **8cRC(u)** at $-44.7 \text{ kcal mol}^{-1}$ (structure type Ib), a stable transition complex **8cTC(u)** at $-70.3 \text{ kcal mol}^{-1}$ (structure type IIa), and a product complex **8cPC(u)** at $-82.3 \text{ kcal mol}^{-1}$ (structure type IIIb), which are separated from each other by a pre- and a post-transition state (see Table 1 and Scheme 2). The pre-transition state could not be optimized because of a nonconverging SCF procedure. However, the post-transition state **8c-postTS(u)** is found at $-68.2 \text{ kcal mol}^{-1}$ (structure type IIIa), which corresponds to a barrier of $2.1 \text{ kcal mol}^{-1}$ for going from the transition complex to the product complex (see Table 1).

Fluorine-Substituent Effects on $S_N2@P$

The origin of the chlorine-substituent effects discussed in the preceding section is primarily the larger steric demand of the chlorine atoms compared to that of the hydrogen atoms. This is consistent with the observed occurrence of steric pre- and/or post-barriers around the stable transition complex in reactions 8 in which both the coordination number and the steric size of the substituents R_1 and R_2 are the largest. Furthermore, the steric origin of such features on the PES has previously been revealed explicitly through activation-strain analyses^[23] along the series of the symmetric reactions of $Cl^- + CH_3Cl$ (1a), $Cl^- + SiH_3Cl$ (2a), $Cl^- + PH_2Cl$ (3a), $Cl^- + POH_2Cl$ (4a), and $Cl^- + PO(CH_3)_2Cl$ (not included in the present set of model reactions).^[7a,8a]

Yet, the increase in electronegativity from $R_1, R_2 = H$ to Cl is likely to have interfered (e.g. through inductive mechanisms) with the steric effects and thus have affected the net result. It is difficult to separate the two effects. To shed some light on how electronegativity influences the observed changes in the reaction profiles, we have compared chlorine with fluorine substitution. Fluorine is also larger than hydrogen, although not as much as chlorine, but it is significantly more electronegative

than the latter. Thus, steric effects will be smaller for fluorine whereas electronegativity effects are amplified to a maximum.

First, we focus on the trend in stability of the transition complexes in the symmetric $S_{\text{N}}2@P4$ reactions with X, Y=Cl: fluorine substitution, that is, on going from **4aTC** (at $-22.3 \text{ kcal mol}^{-1}$) to **6aTC** (at $-13.6 \text{ kcal mol}^{-1}$), a destabilization of the transition complex (by 9 kcal mol^{-1} , see Table 1) is observed. This is still significant but clearly less than the corresponding destabilization (by 14 kcal mol^{-1}) associated with chlorine substitution from **4aTC** to **8aTC**. Thus, when going from reaction 8a (i.e. Cl substitution) to reaction 6a (i.e. F substitution), the transition complex is stabilized by 5 kcal mol^{-1} . In addition, and more strikingly, the pre and post-barriers disappear from reaction 8a to reaction 6a. This remains so also in reaction 6b of $\text{OH}^- + \text{POF}_2\text{OH}$, which features a stable transition complex **6bTC(uu)** that is strongly stabilized by two intramolecular hydrogen bonds (see Table 1). This is very similar to the situation for **8bTC(uu)** (which, as we recall, is labile with respect to the expulsion of a chloride substituent). Apparently, the higher electronegativity of fluorine relative to chlorine substituents does not make up for the somewhat reduced steric bulk in the former. These results support a more prominent role of the steric factors over the electronegativity ones in causing the pre and post-barriers observed upon H/Cl substitution.

With one interesting exception, the above situation is similar for the asymmetric $S_{\text{N}}2@P4$ reactions. If we go from reactions 8c (i.e. Cl substitution) to the corresponding asymmetric $S_{\text{N}}2@P4$ reaction 6c (i.e., F substitution), the pre-barrier disappears (see Tables 1 and 2). Note, however, that the post-barrier remains intact, although it has been reduced to only $0.1 \text{ kcal mol}^{-1}$. This yields a double-well PES, as shown in Figure 1E. In the initial product complex **6cPC(u)**, the expelled Cl^- leaving group coordinates to the hydroxy oxygen and the fluorine substituents, collinear with the P=O bond (structure type IIIc in Scheme 2). Product complex **6cPC(u)** is only weakly bound (by $-3.8 \text{ kcal mol}^{-1}$) regarding its dissociation into the final products $\text{POF}_2\text{OH} + \text{Cl}^-$ (see Table 1). Alternatively, it may rearrange to form a more stable complex, **6cPC(u)-alt**, in which Cl^- forms a hydrogen bond of $-37.0 \text{ kcal mol}^{-1}$ with the OH group ($\text{POF}_2\text{O}-\text{H}\cdots\text{Cl}^-$, structure type IIIId in Scheme 2; see also Table S1 of the Supporting Information). This supports, again, a more prominent role of the steric factors in causing the pre- and post-barriers and thus the triple-well PES.

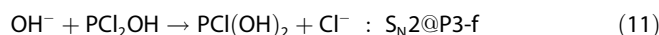
Effect of the Hydroxy Conformation on $S_{\text{N}}2@P$

The OH groups in the $S_{\text{N}}2@P3$ and $S_{\text{N}}2@P4$ reactions involving hydroxide as the leaving group and/or nucleophile can, as already mentioned above, adopt different orientations. In most—but not all—cases, these orientations can give rise to different stable conformers and thus to different pathways (see Scheme 1). So far, we have focused on the lowest-energy pathways corresponding to stationary points with the most stable conformations. Here, we briefly discuss the other conformers that constitute the higher-energy pathways.

We begin with the $S_{\text{N}}2@P3$ reactions. For reaction 3b of $\text{OH}^- + \text{PH}_2\text{OH}$, the most stable transition complex is **3bTC(uu)**,

that is, both O–H bonds pointing “up” (see Scheme 1). Switching one or both OH groups downwards, that is, going from **3bTC(uu)** to **3bTC(du)** and finally to **3bTC(dd)**, leads in each of the two steps to an energy rise of $1.2 \text{ kcal mol}^{-1}$ (see Table S1 of the Supporting Information). This is ascribed to an increase in the steric repulsion between the O–H and P–H bonds (see ref. [24]). On the other hand, for the $S_{\text{N}}2@P3$ reactions 5b and 7b, the most stable conformation is with the O–H bonds pointing downwards, that is, towards the electronegative fluorine and chlorine substituents, respectively. This is ascribed to the possibility to form intramolecular hydrogen bonds of the type $\text{O}-\text{H}\cdots\text{R}$ with $\text{R}=\text{F}$ or Cl . Thus, when switching one or two OH groups upwards along **5bTC(dd)**, **5bTC(ud)**, and **5bTC(uu)**, the energy of the transition complex goes up by 1.5 and $1.6 \text{ kcal mol}^{-1}$, respectively (see Table S1 of the Supporting Information).

Interestingly, **7bTC(dd)** is the only stable conformer for the transition complex resulting from $\text{OH}^- + \text{PCl}_2\text{OH}$. Thus, the regular backside $S_{\text{N}}2@P3$ reaction 7b only occurs if OH^- is oriented “d” as it approaches PCl_2OH . Alternatively, if OH^- approaches in a “u”-oriented fashion (and/or if the substrate itself is in the “s” conformation **7bR(s)** which is $2.8 \text{ kcal mol}^{-1}$ above **7bR(d)**, see Table S1 of the Supporting Information), a chloride substituent acts as a leaving group and is spontaneously expelled. This corresponds overall to a barrierless frontside $S_{\text{N}}2@P3$ reaction, designated by $S_{\text{N}}2@P3\text{-f}$ [Eq. (11); see also entry 7b'' in Table 3]:



This process leads initially to a very stable $\text{PCl}(\text{OH})_2\cdots\text{Cl}^-$ complex, **7bPC(η^2)-f** (at $-100.2 \text{ kcal mol}^{-1}$, see Table 3), in which the $\text{PCl}(\text{OH})_2$ unit binds dihapto, that is, through its two O–H bonds, with Cl^- (structure type Vb in Scheme 2). Overall, reaction 11 is $-64.2 \text{ kcal mol}^{-1}$ exothermic (see Table S1 of the Supporting Information). The same overall transformation can also proceed via the stable transition complex **7bTC(dd)** (structure type IIa in Scheme 2), but proceeding from the latter, a small barrier of $0.3 \text{ kcal mol}^{-1}$ (provided by **7bTS(dd)-f**, see Table S1 of the Supporting Information) must be surmounted before the chloride leaving group can be expelled.

In the $S_{\text{N}}2@P4$ reactions 4b, 6b, and 8b, the most stable orientation for the O–H bonds is “u” because of the intramolecular hydrogen bonds with the phosphoryl oxygen atom. In fact, for $S_{\text{N}}2@P4$ reaction 4b of $\text{OH}^- + \text{POH}_2\text{OH}$, the only stable transition complex is **4bTC(uu)** (structure type IIa in Scheme 2). All other conformations reorient spontaneously to the one in this transition complex. On the other hand, for reactions 6b and 8b, other conformations have been found with either one or two O–H bonds pointing “down”. Thus, switching one or both OH groups downwards, that is, going from **6bTC(uu)** to **6bTC(du)** to **6bTC(dd)**, causes the energy to increase first by $2.3 \text{ kcal mol}^{-1}$ and then by another $2.6 \text{ kcal mol}^{-1}$ (see Scheme 1 and Table S1 of the Supporting Information).

In the case of the transition complexes **5bTC(dd)**, **6bTC(uu)**, and **7bTC(dd)**, we note that interchanging axial (i.e. $X=Y=\text{OH}$) and equatorial positions (i.e. $\text{R}_1=\text{R}_2=\text{F}$, F and Cl respec-

Table 4. Geometry parameters [\AA , degrees] of selected stationary points of the frontside $S_{\text{N}}2@P$ process and other alternative pathways to reactions 3–8, with OH^- as the nucleophile.^[a]

Species	Type ^[b]	$R_{1,2}$ ^[c]	X-P	P-Y	P- R_1 ^[d]	P- R_2 ^[e]	X- R_1 ^[f]	X-P-Y
3bTS(uu)-f	IV	H	1.69	1.69	4.11	1.42	5.23	104
3bPC-f	VI	H	1.54	1.74	4.16	1.51	0.75 (2.52)	106
4bTS1(ss)-f	IIa	H	1.78	1.78	1.46	1.43	2.15	143
4bTC2(ss)-f	IIb	H	1.73	1.73	1.50	1.44	1.98	120
4bTS2(ss)-f	IV	H	1.65	1.65	2.09	1.43	1.70	114
4bPC-f	VI	H	1.51	1.69	4.54	1.44	0.75 (2.95)	106
5bTS(dd)-f	IV	F	1.72	1.72	2.05	1.67	1.87	146
5bPC-f	VI	F	1.54	1.69	3.59	1.69	1.02 (1.44)	105
6bTS(uu)-f	IV	F	1.59	1.60	3.02	1.56	2.85	110
6bPC-f	VI	F	1.50	1.65	3.73	1.62	0.98 (1.54)	108
6cTS1(s)-f	IIa	F	1.69	2.32	1.67	1.63	2.15	149
6cTC2(s)-f	IIb	F	1.65	2.15	1.77	1.67	1.93	115
6cTS2(s)-f	IV	F	1.60	2.09	2.13	1.64	1.52	112
6cPC-f	VI	F	1.50	2.11	3.85	1.61	0.97 (1.60)	107
7bTS(dd)-f	IV	Cl	1.73	1.73	2.44	2.26	2.55	165
7bPC(η^2)-f	Vb	Cl	1.61	1.61	3.70	2.23	2.03 (1.02)	104
7bTC-alt	IIb	Cl	1.66	1.66	2.47	2.47	2.35	104
7bTS-f/alt	IV	Cl	1.66	1.66	2.64	2.35	2.25	104
7bPC(η^1)-f	Va	Cl	1.57	1.66	3.85	2.23	1.68 (1.13)	101
8bPC(η^1)-f	Va	Cl	1.51	1.63	3.89	2.12	1.49 (1.31)	107
8bTS(η^1/η^2)-f	Va	Cl	1.54	1.63	3.75	2.08	1.63 (1.16)	109
8bPC(η^2)-f	Vb	Cl	1.58	1.58	3.60	2.10	1.98 (1.02)	107
8cTS(s)-f	IV	Cl	1.69	2.36	2.18	2.13	2.72	163
8cPC-alt	IIIe	Cl	1.50	2.10	4.09	2.10	1.39 (1.50)	107

[a] Computed at the OLYP/TZ2P level. See Table 3 for relative energies. [b] Generic types of stationary points (see Schemes 1 and 2). [c] See Scheme 1 for a perspective that defines R_1 and R_2 . [d] Distance to the frontside leaving group R_1 . [e] Distance to the nonleaving R_2 . [f] Shortest distance between X (=OH) and R_1 . For product complexes, the O–H distance in X (=OH) is shown in parentheses to indicate whether a proton-transfer has occurred.

tively), that is, going from structure type IIa to IIb in Scheme 2, causes a substantial stabilization of -14 , -12 , and -34 kcal mol $^{-1}$, respectively (see **5bTC-alt**, **6bTC-alt**, and **7bTC-alt** in Table S1 of the Supporting Information). These species are, however, not located directly on the routes of the $S_{\text{N}}2@P$ pathways that start from reactants in their most stable conformation. Instead, they may proceed from the substrate in a higher energy conformation.

We have fully explored such pathways for the case of an OH^- ion attacking the neutral molecule **7bR(s)**, in which the OH group of PCl_2OH is oriented sideways instead of downwards, as in the more stable (by -2.8 kcal mol $^{-1}$) **7bR(d)** species (see Table 3 and Scheme 1). This gives rise to the following alternatives to the back- and frontside channels of reaction 7b (see Table 3): i) the stable **7bTC-alt** species is formed in reactions 7b' in which **7bR(s)** is attacked by an "s"-oriented OH^- ion that points to a direction opposite to that of the OH group in the substrate; ii) the product complex **7bPC(η^2)-f** (structure type Vb in Scheme 2) is formed in reaction 7b'' which covers all other orientations of the incoming OH^- species. The transition complex **7bTC-alt** of reactions 7b' can either dissociate into the backside $S_{\text{N}}2@P3$ products **7bP(d)** + OH^- (this is a nearly, but not exactly, thermoneutral process), or into the frontside $S_{\text{N}}2@P3$ -f products **7bP-f/alt** + Cl^- (this is an exothermic process involving an energy of -67.1 kcal mol $^{-1}$, see Table 3). Note that the backside $S_{\text{N}}2@P3$ reaction 7b' is slightly

exothermic (-2.8 kcal mol $^{-1}$), and not exactly thermoneutral as the backside $S_{\text{N}}2@P3$ reaction 7b, because the substrate of reaction 7b' is in a conformation that is higher in energy (exactly by the above-mentioned amount of 2.8 kcal mol $^{-1}$) than the ground-state conformation.

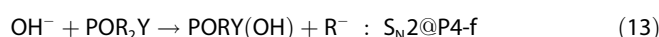
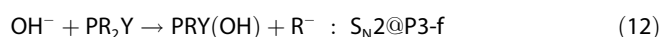
In conclusion, the $S_{\text{N}}2@P3$ and $S_{\text{N}}2@P4$ reactions involving hydroxide as the leaving group and/or nucleophile can, depending on the orientations of the O–H bonds, proceed via parallel backside $S_{\text{N}}2$ pathways that are 1 to 5 kcal mol $^{-1}$ above the lowest-energy pathway, or they may deviate into alternative mechanistic pathways (e.g. reaction 7b which is redirected toward reaction 11).

Frontside $S_{\text{N}}2@P$ and Other Alternative Elimination Pathways

We have discussed the regular backside $S_{\text{N}}2@P$ pathways 3–8 of our model reaction systems, the substituent effects thereon,

and the dependence of the reactions on OH-group conformations. In some of the hydroxide-induced processes, we encountered competing reaction channels leading to the frontside $S_{\text{N}}2@P$ process in which one of the substituents R plays the role of the leaving group. This has prompted us to carry out a more systematic study of the front- versus backside $S_{\text{N}}2@P$ competition for reactions 3b–8b (i.e. $X=Y=\text{OH}$) and a few others (see Tables 3 and 4 and Scheme 2).

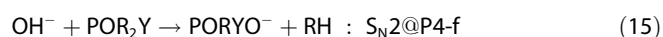
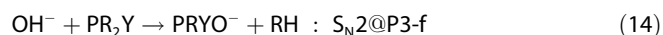
The simple frontside $S_{\text{N}}2@P3$ -f and $S_{\text{N}}2@P4$ -f reactions [see Eqs. (12) and (13)] are—both thermodynamically and kinetically—either comparable to, or significantly more favorable than, the corresponding backside pathways (compare "front" with "back" in Table 3).



Hydride is, not unexpectedly, the worst and chloride the best among the frontside leaving groups studied here. Thus, the reaction energies of both $S_{\text{N}}2@P3$ -f ($\Delta E = 2.3$, -13.2 , and -64.2 kcal mol $^{-1}$ for 3b, 5b, and 7b) and $S_{\text{N}}2@P4$ -f ($\Delta E = -8.1$, -17.9 , and -70.2 kcal mol $^{-1}$ for 4b, 6b, and 8b) become more exothermic as the frontside leaving group varies along $R = \text{H, F, Cl}$ (see Table 3). These frontside pathways are thermodynamically competitive with the corresponding backside $S_{\text{N}}2@P3$

and $S_{\text{N}}2@P4$ reactions involving the hydroxide ($Y=OH$) leaving group, which are all thermoneutral (see Table 3).

In most cases, the frontside pathway proceeds via one or more barriers on the PES (see Table 3). This holds, for example, for reactions 3b–7b (and also for 6c and 8c, which are not further discussed), but not for reaction 8b. The frontside pathway of the latter is, as discussed above, spontaneously accessed once the pre-barrier towards the labile transition complex **8bTC**(uu) is crossed [see Eq. (10) in Section “Chlorine-Substituent Effects on $S_{\text{N}}2@P$ ”]. In all cases, the intermediates and transition states on the PES are (significantly) more stable than the products of the regular backside $S_{\text{N}}2@P$ reactions (see Table 3):



Interestingly, the hydride and fluoride leaving groups in the frontside pathways of reactions 3b–6b are basic enough to abstract a proton from an OH group in the product molecule anticipated for the frontside $S_{\text{N}}2@P$ process. These alternative channels to reactions 3b–6b lead to the elimination of molecular hydrogen or hydrogen fluoride [see Eqs. (14) and (15) above] and are overall exothermic (by -54 to -82 kcal mol $^{-1}$, see Table 3).

Conclusions

Nucleophilic substitution at the tri- and tetracoordinate phosphorus centers of the model reactions $X^- + \text{PH}_2\text{Y}$ ($S_{\text{N}}2@P3$) and $X^- + \text{POH}_2\text{Y}$ ($S_{\text{N}}2@P4$) is characterized by single-well reaction profiles with a stable, hypervalent transition complex (TC), similar to nucleophilic substitution at silicon ($S_{\text{N}}2@Si$). Differences between $S_{\text{N}}2@P3$ and $S_{\text{N}}2@P4$ are minor. However, the $S_{\text{N}}2@P4$ substitution (unlike $S_{\text{N}}2@P3$) exhibits a characteristic behavior, which is also observed in $S_{\text{N}}2@Si$: introducing sufficient steric bulk around the central atom causes the appearance of pre- and post-barriers that separate the TC from the reactant and product complexes. These extra features along the PES appear to be preserved also when the reaction becomes significantly exothermic (e.g. -71 kcal mol $^{-1}$ for $\text{OH}^- + \text{POCl}_3$).

An interesting feature of $S_{\text{N}}2@P$ reactions involving an OH^- nucleophile and/or leaving group is the existence of reaction channels, occurring in parallel, that differ in the conformation of the OH groups. Parallel reaction channels may lead to the same but, in some cases, also to different products.

Finally, the backside $S_{\text{N}}2@P$ reaction is found to compete with thermodynamically favorable frontside pathways (i.e. $S_{\text{N}}2@P\text{-f}$), in which one of the other substituents at P, instead of the anticipated leaving group Y, is expelled. The $S_{\text{N}}2@P\text{-f}$ pathway may also lead to the elimination of H_2 or HF if the substituent that is expelled in the substitution step is a sufficiently strong base (i.e. H or F) to abstract a proton from an OH group in the initial product molecule.

Acknowledgements

We thank the National Research School Combination—Catalysis (NRSC-C) and the Netherlands Organization for Scientific Research (NWO-CW and NWO-NCF) for financial support.

Keywords: density functional calculations · hypervalence · nucleophilic substitution · phosphorus · reaction mechanisms

- [1] J. March, *Advanced Organic Chemistry*, 4th ed., Wiley-Interscience, New York, 1992.
- [2] P. Walden, *Ber. Dtsch. Chem. Ges.* **1893**, 26, 210–215.
- [3] a) S. Gronert, *Acc. Chem. Res.* **2003**, 36, 848–857; b) S. Gronert, *Chem. Rev.* **2001**, 101, 329–360; c) C. Li, P. Ross, J. E. Szulejko, T. B. McMahon, *J. Am. Chem. Soc.* **1996**, 118, 9360–9367; d) C. H. DePuy, S. Gronert, A. Mullin, V. M. Bierbaum, *J. Am. Chem. Soc.* **1990**, 112, 8650–8655; e) S. E. Barlow, J. M. Van Doren, V. M. Bierbaum, *J. Am. Chem. Soc.* **1988**, 110, 7240–7242; f) W. N. Olmstead, J. I. Brauman, *J. Am. Chem. Soc.* **1977**, 99, 4219–4228.
- [4] a) E. Uggerud, *Chem. Eur. J.* **2006**, 12, 1127–1136; b) A. P. Bento, M. Solà, F. M. Bickelhaupt, *J. Comput. Chem.* **2005**, 26, 1497–1504; c) J. M. Gonzales, W. D. Allen, H. F. Schaefer III, *J. Phys. Chem. A* **2005**, 109, 10613–10628; d) S. Schmatz, *ChemPhysChem* **2004**, 5, 600–617; e) G. Vayner, K. N. Houk, W. L. Jorgensen, J. I. Brauman, *J. Am. Chem. Soc.* **2004**, 126, 9054–9058; f) J. M. Gonzales, C. Pak, R. S. Cox, W. D. Allen, H. F. Schaefer III, A. G. Csaszar, G. Tarczay, *Chem. Eur. J.* **2003**, 9, 2173–2192; g) J. K. Laerdahl, E. Uggerud, *Int. J. Mass Spectrom.* **2002**, 214, 277–314; h) I. Lee, C. K. Kim, C. K. Sohn, H. G. Li, H. W. Lee, *J. Phys. Chem. A* **2002**, 106, 1081–1087; i) Y. A. Borisov, E. E. Arcia, S. L. Mielke, B. C. Garrett, T. H. Dunning, *J. Phys. Chem. A* **2001**, 105, 7724–7736; j) F. M. Bickelhaupt, *J. Comput. Chem.* **1999**, 20, 114–128; k) P. Botschwina, *Theor. Chem. Acc.* **1998**, 99, 426–428; l) M. L. Chabinyk, S. L. Craig, C. K. Regan, J. I. Brauman, *Science* **1998**, 279, 1882–1886; m) S. Harder, A. Streitwieser, J. T. Petty, P. v. R. Schleyer, *J. Am. Chem. Soc.* **1995**, 117, 3253–3259; n) W. L. Hase, *Science* **1994**, 266, 998–1002; o) M. N. Glukhovtsev, A. Pross, L. Radom, *J. Am. Chem. Soc.* **1995**, 117, 2024–2032; p) L. Q. Deng, V. Brachadell, T. Ziegler, *J. Am. Chem. Soc.* **1994**, 116, 10645–10656; q) F. M. Bickelhaupt, E. J. Baerends, N. M. M. Nibbering, T. Ziegler, *J. Am. Chem. Soc.* **1993**, 115, 9160–9173; r) S. S. Shaik, H. B. Schlegel, S. Wolfe, *Theoretical Aspects of Physical Organic Chemistry: The $S_{\text{N}}2$ Reaction*, Wiley, New York, 1992; s) J. D. Evanseck, J. F. Blake, W. L. Jorgensen, *J. Am. Chem. Soc.* **1987**, 109, 2349–2353; t) J. Chandrasekhar, S. F. Smith, W. L. Jorgensen, *J. Am. Chem. Soc.* **1985**, 107, 154–163; u) K. Ohta, K. Morokuma, *J. Phys. Chem.* **1985**, 89, 5845–5849; v) H. B. Schlegel, K. Mislow, F. Bernardi, A. Bottoni, *Theor. Chim. Acta* **1977**, 44, 245–256.
- [5] J. I. Brauman, *J. Mass Spectrom.* **1995**, 30, 1649–1651.
- [6] a) M. N. Glukhovtsev, A. Pross, L. Radom, *J. Am. Chem. Soc.* **1995**, 117, 9012–9018; b) P. Beak, J. L. Li, *J. Am. Chem. Soc.* **1991**, 113, 2796–2797.
- [7] a) A. P. Bento, F. M. Bickelhaupt, *J. Org. Chem.* **2007**, 72, 2201–2207; b) R. R. Holmes, *Chem. Rev.* **1996**, 96, 927–950; c) R. Damrauer, J. A. Hankin, *Chem. Rev.* **1995**, 95, 1137–1160; d) T. L. Windus, M. S. Gordon, L. P. Davis, L. W. Burggraf, *J. Am. Chem. Soc.* **1994**, 116, 3568–3579; e) M. T. Carroll, M. S. Gordon, T. L. Windus, *Inorg. Chem.* **1992**, 31, 825–829; f) Z. Shi, R. J. Boyd, *J. Phys. Chem.* **1991**, 95, 4698–4701; g) R. R. Holmes, *Chem. Rev.* **1990**, 90, 17–31; h) S. Gronert, R. Glaser, A. Streitwieser, *J. Am. Chem. Soc.* **1989**, 111, 3111–3117; i) R. Damrauer, L. W. Burggraf, L. P. Davis, M. S. Gordon, *J. Am. Chem. Soc.* **1988**, 110, 6601–6606; j) D. J. Hajdasz, R. R. Squires, *J. Am. Chem. Soc.* **1986**, 108, 3139–3140; k) J. C. Sheldon, R. N. Hayes, J. H. Bowie, *J. Am. Chem. Soc.* **1984**, 106, 7711–7715; l) M. J. S. Dewar, E. Healy, *Organometallics* **1982**, 1, 1705–1708; m) R. L. Hilderbrandt, G. D. Homer, P. Boudjouk, *J. Am. Chem. Soc.* **1976**, 98, 7476–7480; n) P. Baybutt, *Mol. Phys.* **1975**, 29, 389–403; o) L. H. Sommer, G. A. Parker, N. C. Lloyd, C. L. Frye, K. W. Michael, *J. Am. Chem. Soc.* **1967**, 89, 857–861; p) L. H. Sommer, *Stereochemistry, Mechanism, and Silicon*, McGraw-Hill, New York, 1965.
- [8] a) M. A. van Bochove, M. Swart, F. M. Bickelhaupt, *J. Am. Chem. Soc.* **2006**, 128, 10738–10744; b) T. I. Sølling, A. Pross, L. Radom, *Int. J. Mass*

- Spectrom.* **2001**, *210*, 1–11; c) S. M. Bachrach, D. C. Mulhearn, *J. Phys. Chem.* **1993**, *97*, 12229–12231.
- [9] a) D. E. C. Corbridge, *Phosphorus 2000: Chemistry, Biochemistry & Technology*, Elsevier, Amsterdam, **2000**; b) A. J. Kirby, S. G. Warren, *The Organic Chemistry of Phosphorus*, Elsevier, Amsterdam, **1967**.
- [10] a) C. Fish, M. Green, R. J. Kilby, J. M. Lynam, J. E. McGrady, D. A. Pantazis, C. A. Russell, A. C. Whitwood, C. E. Willans, *Angew. Chem.* **2006**, *118*, 3710–3713; *Angew. Chem. Int. Ed.* **2006**, *45*, 3628–3631; b) K. C. Kumara Swamy, N. Satish Kumar, *Acc. Chem. Res.* **2006**, *39*, 324–333; c) A. C. Hengge, I. Onyido, *Curr. Org. Chem.* **2005**, *9*, 61–74; d) R. R. Holmes, *Acc. Chem. Res.* **2004**, *37*, 746–753; e) O. S. Lee, K. Yang, K. D. Kang, I. S. Koo, C. K. Kim, I. Lee, *J. Comput. Chem.* **2004**, *25*, 1740–1748; f) K. Range, M. J. McGrath, X. Lopez, D. M. York, *J. Am. Chem. Soc.* **2004**, *126*, 1654–1665; g) S. Humbel, C. Bertrand, C. Darcel, C. Bauduin, S. Juge, *Inorg. Chem.* **2003**, *42*, 420–427; h) S. D. Lahiri, G. Zhang, D. Dunaway-Mariano, K. N. Allen, *Science* **2003**, *299*, 2067–2071; see also: G. M. Blackburn, N. H. Williams, S. J. Gamblin, S. J. Smerdon, *Science* **2003**, *301*, 1184c and K. N. Allen, D. Dunaway-Mariano, *Science* **2003**, *301*, 1184d; i) R. E. Hanes, Jr., V. M. Lynch, E. V. Anslin, K. N. Dalby, *Org. Lett.* **2002**, *4*, 201–203; j) N. Y. Chang, C. Lim, *J. Am. Chem. Soc.* **1998**, *120*, 2156–2167; k) J. Florian, A. Warshel, *J. Phys. Chem. B* **1998**, *102*, 719–734; l) N. Y. Chang, C. Lim, *J. Phys. Chem. A* **1997**, *101*, 8706–8713; m) J. Florian, A. Warshel, *J. Am. Chem. Soc.* **1997**, *119*, 5473–5474; n) P. Tole, C. M. Lim, *J. Phys. Chem.* **1993**, *97*, 6212–6219; o) A. Yliniemela, T. Uchimaru, K. Tanabe, K. Taira, *J. Am. Chem. Soc.* **1993**, *115*, 3032–3033; p) J. L. Li, P. Beak, *J. Am. Chem. Soc.* **1992**, *114*, 9206–9207; q) R. C. Lum, J. J. Grabowski, *J. Am. Chem. Soc.* **1992**, *114*, 8619–8627; r) C. Lim, M. Karplus, *J. Am. Chem. Soc.* **1990**, *112*, 5872–5873; s) R. V. Hodges, S. A. Sullivan, J. L. Beauchamp, *J. Am. Chem. Soc.* **1980**, *102*, 935–938; t) M. Mikolajczyk, J. Omelanczuk, W. Perlikowska, *Tetrahedron* **1979**, *35*, 1531–1536; u) O. I. Asubiojo, J. I. Brauman, R. H. Levin, *J. Am. Chem. Soc.* **1977**, *99*, 7707–7708; v) E. P. Kyba, *J. Am. Chem. Soc.* **1976**, *98*, 4805–4809; w) E. P. Kyba, *J. Am. Chem. Soc.* **1975**, *97*, 2554–2555; x) R. D. Cook, C. E. Diebert, W. Schwarz, P. C. Turley, P. Haake, *J. Am. Chem. Soc.* **1973**, *95*, 8088–8096.
- [11] a) E. Skordalakes, G. G. Dodson, D. St Clair-Green, C. A. Goodwin, M. F. Scully, H. R. Hudson, V. V. Kakkar, J. J. Deadman, *J. Mol. Biol.* **2001**, *311*, 549–555; b) J. E. Omakor, I. Onyido, G. W. van Loon, E. Buncel, *J. Chem. Soc. Perkin Trans. 2* **2001**, 324–330; c) M. Oivanen, S. Kuusela, H. Lönnberg, *Chem. Rev.* **1998**, *98*, 961–990; d) D. M. Perreault, E. V. Anslin, *Angew. Chem.* **1997**, *109*, 470–490; *Angew. Chem. Int. Ed. Engl.* **1997**, *36*, 432–450; e) M. R. Sawaya, R. Prasad, S. H. Wilson, J. Kraut, H. Pelletier, *Biochemistry* **1997**, *36*, 11205–11215; f) J. M. Denu, D. L. Lohse, J. Vijayalakshmi, M. A. Saper, J. E. Dixon, *Proc. Natl. Acad. Sci. USA* **1996**, *93*, 2493–2498; g) F. H. Westheimer, *Science* **1987**, *235*, 1173–1178; h) N. Iché-Tarrat, M. Ruiz-Lopez, J.-C. Barthelat, A. Vigroux, *Chem. Eur. J.* **2007**, *13*, 3617–3629; i) J. Wang, J. Gu, J. Leszczynski, M. Feliks, W. A. Sokalski, *J. Phys. Chem. B* **2007**, *111*, 2404–2408; j) J. Šečková, J. L. Menke, R. J. Emmett, E. V. Patterson, C. J. Cramer, *J. Org. Chem.* **2005**, *70*, 8649–8660; k) F. Zheng, C.-G. Zhan, R. L. Ornstein, *J. Chem. Soc. Perkin Trans. 2* **2001**, 2355–2363.
- [12] a) R. G. Parr, W. Yang, *Density Functional Theory of Atoms and Molecules*, Oxford University Press, New York, **1989**; b) W. Koch, M. C. Holthausen, *A Chemist's Guide to Density Functional Theory*, Wiley-VCH, Weinheim, **2000**; c) R. Dreizler, E. Gross, *Density Functional Theory*, Plenum, New York, **1995**; d) F. M. Bickelhaupt, E. J. Baerends, *Rev. Comput. Chem.* **2000**, *15*, 1–86; e) E. J. Baerends, O. V. Gritsenko, *J. Phys. Chem. A* **1997**, *101*, 5383–5403; f) T. Ziegler, *Can. J. Chem.* **1995**, *73*, 743–761; g) T. Ziegler, *Chem. Rev.* **1991**, *91*, 651–667.
- [13] a) N. C. Handy, A. J. Cohen, *J. Chem. Phys.* **2002**, *116*, 5411–5418; b) N. C. Handy, A. J. Cohen, *Mol. Phys.* **2001**, *99*, 403–412; c) C. T. Lee, W. T. Yang, R. G. Parr, *Phys. Rev. B* **1988**, *37*, 785–789.
- [14] M. Swart, M. Solà, F. M. Bickelhaupt, *J. Comput. Chem.* **2007**, *28*, 1551–1560.
- [15] a) E. J. Baerends, J. Autschbach, A. Bérces, F. M. Bickelhaupt, C. Bo, P. M. Boerrigter, L. Cavallo, D. P. Chong, L. Deng, R. M. Dickson, D. E. Ellis, M. van Faassen, L. Fan, T. H. Fischer, C. Fonseca Guerra, S. J. A. van Gisbergen, J. A. Groeneveld, O. V. Gritsenko, M. Grüning, F. E. Harris, P. van den Hoek, C. R. Jacob, H. Jacobsen, L. Jensen, G. van Kessel, F. Kootstra, E. van Lenthe, D. A. McCormack, A. Michalak, J. Neugebauer, V. P. Osinga, S. Patchkovskii, P. H. T. Philipsen, D. Post, C. C. Pye, W. Ravenek, P. Ros, P. R. T. Schipper, G. Schreckenbach, J. G. Snijders, M. Solà, M. Swart, D. Swerhone, G. te Velde, P. Vernooijs, L. Versluis, L. Visscher, O. Visser, F. Wang, T. A. Wesolowski, E. M. van Wezenbeek, G. Wiesenekker, S. K. Wolff, T. K. Woo, A. L. Yakovlev, T. Ziegler, ADF version 2005.01 and 2006.01, SCM, Amsterdam, The Netherlands; b) G. te Velde, F. M. Bickelhaupt, E. J. Baerends, C. Fonseca Guerra, S. J. A. van Gisbergen, J. G. Snijders, T. Ziegler, *J. Comput. Chem.* **2001**, *22*, 931–967; c) E. J. Baerends, D. E. Ellis, P. Ros, *Chem. Phys.* **1973**, *2*, 41–51; d) C. Fonseca Guerra, J. G. Snijders, G. te Velde, E. J. Baerends, *Theor. Chem. Acc.* **1998**, *99*, 391–403.
- [16] a) M. Swart, A. W. Ehlers, K. Lammertsma, *Mol. Phys.* **2004**, *102*, 2467–2474; b) J. Baker, P. Pulay, *J. Chem. Phys.* **2002**, *117*, 1441–1449; c) X. Xu, W. A. Goddard III, *J. Phys. Chem. A* **2004**, *108*, 8495–8504.
- [17] a) M. Grüning, O. V. Gritsenko, E. J. Baerends, *J. Phys. Chem. A* **2004**, *108*, 4459–4469; b) O. V. Gritsenko, B. Ensing, P. R. T. Schipper, E. J. Baerends, *J. Phys. Chem. A* **2000**, *104*, 8558–8565.
- [18] E. van Lenthe, E. J. Baerends, *J. Comput. Chem.* **2003**, *24*, 1142–1156.
- [19] a) F. Jensen, *Introduction to Computational Chemistry*, Wiley, New York, **1998**; b) L. Fan, T. Ziegler, *J. Chem. Phys.* **1990**, *92*, 3645–3652; c) L. Y. Fan, L. Versluis, T. Ziegler, E. J. Baerends, W. Ravenek, *Int. J. Quantum Chem.* **1988**, 173–181.
- [20] The precise value of the reactive-cone angle varies somewhat with the orientation of the OH⁻ group with respect to the substrate. We have not fully explored this dependence.
- [21] a) M. Swart, F. M. Bickelhaupt, *J. Chem. Theory Comput.* **2006**, *2*, 281–287; see also b) M. Swart, E. Rösler, F. M. Bickelhaupt, *Eur. J. Inorg. Chem.* **2007**, 3646–3654.
- [22] See, for example: a) D. Hugas, S. Simon, M. Duran, *J. Phys. Chem. A* **2007**, *111*, 4506–4512; b) D. Hugas, S. Simon, M. Duran, *Chem. Phys. Lett.* **2004**, *386*, 373–376.
- [23] G. Th. de Jong, F. M. Bickelhaupt, *ChemPhysChem* **2007**, *8*, 1170–1181.
- [24] For the role of steric repulsion in the conformational preferences, see, for example: a) F. M. Bickelhaupt, E. J. Baerends, *Angew. Chem.* **2003**, *115*, 4315–4320; *Angew. Chem. Int. Ed.* **2003**, *42*, 4183–4188; b) J. Poater, M. Solà, F. M. Bickelhaupt, *Chem. Eur. J.* **2006**, *12*, 2889–2895.
- [25] The energy of the second-order saddle point **3bTS(uu)-f** is an upper bound for that of the real transition state. TS optimization unavoidably yields the species **3bTS(uu)-f**, which has two normal modes with imaginary frequencies instead of one. The larger imaginary frequency (73i cm⁻¹) corresponds to the H⁻ species moving away from P, while the smaller imaginary frequency (41i cm⁻¹) corresponds to H⁻ moving sideways, towards an OH group.

Received: July 19, 2007

Revised: September 9, 2007

Published online on November 7, 2007